Research Article

Electrochemical measurements of synthesized nanostructured β-Ni(OH)$_2$ using hydrothermal process and activated carbon based nanoelectroactive materials

S. Kettaf[1] · O. Guellati[1,2] · A. Harat[1] · H. Kennaz[1] · D. Momodu[3] · J. Dangbegnon[3] · N. Manyala[3] · M. Guerioune[1]

Abstract

In this investigation, nickel hydroxide Ni(OH)$_2$ based nanostructured materials were synthesized by simple and low cost free template hydrothermal method at two different growth temperatures with and without SDS surfactant. The X-ray diffraction, Raman spectroscopy and field emission scanning electron microscopy analysis confirmed the formation of β-Ni(OH)$_2$ pure brucite crystalline phase in spherical nanoparticle morphology with an average diameter ranging from 8 to 27 nm. In the second step, these nanospherical agglomerated hydroxide particles with activated carbon addition were performed as electroactive materials deposited on nickel foam current collector as working electrodes. The electrochemical tests in a three-electrode configuration using 6 MKOH electrolyte show that the best electroactive NPs (β_{bc}-Ni(OH)$_2$ and β-Ni(OH)$_2$ obtained at optimized conditions, have a maximum specific capacitance (C_s) of 4697 F g^{-1} and 3431 F g^{-1} at 5 mV s^{-1} scan rate with a specific capacity (Q_s) of 744 mAh g^{-1} and 618 mAh g^{-1} at 1 A g^{-1} current density with an R_s of about 0.24 and 0.28 Ω, respectively. At 30 A g^{-1} after 1700 cycles, the coulombic retention is around 99.06% (or capacity retention 109 mAh g^{-1}), demonstrating remarkable cycling stability for Ni based hydroxide.

✉ O. Guellati, guellati23@yahoo.fr | [1]LEREC Laboratory, Physic Department, Badji Mokhtar University of Annaba, BP. 12, 23000 Annaba, Algeria. [2]Mohamed Chérif Messaadia University of Souk-Ahras, BP. 1553, 41000 Souk Ahras, Algeria. [3]Department of Physics, Institute of Applied Materials, SARChI Chair in Carbon Technology and Materials, University of Pretoria, Pretoria 0028, South Africa.

SN Applied Sciences (2019) 1:34 | https://doi.org/10.1007/s42452-018-0038-3

Received: 13 July 2018 / Accepted: 29 October 2018

Published online: 05 November 2018

SN Applied Sciences
A SPRINGER NATURE journal

Graphical abstract

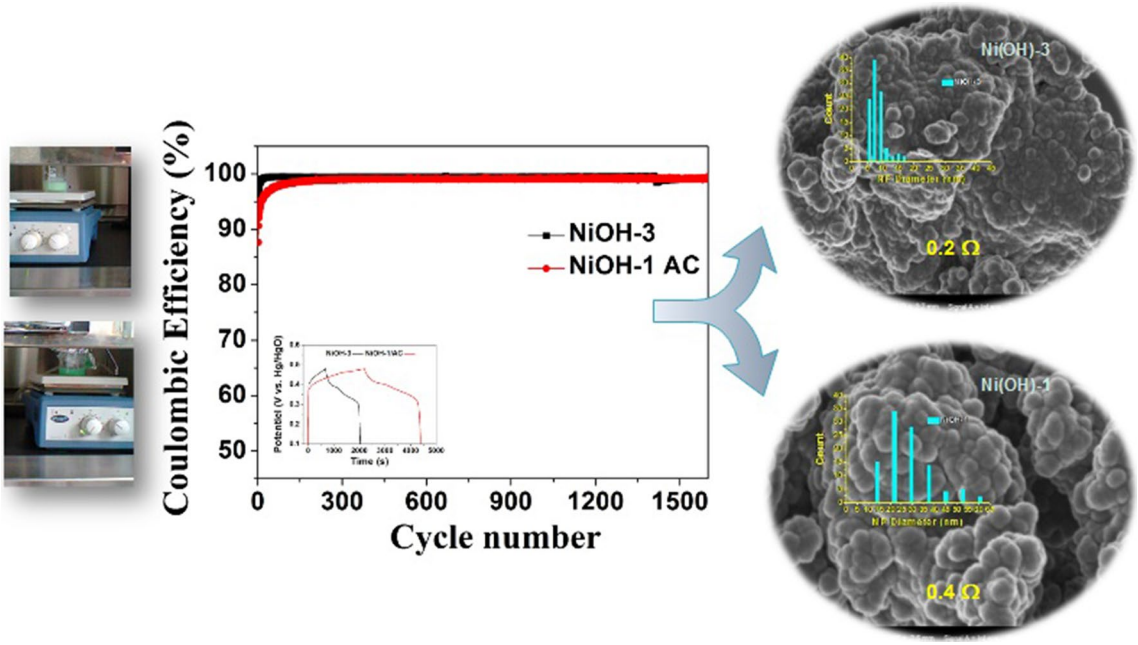

Keywords Nickel hydroxide · Activated carbon · Hydrothermal process · Electrochemical performance · Supercapacitors

1 Introduction

Transition metal hydroxides and oxides at nanoscale with different morphologies such as nanoparticles, nanowires, nanotubes, nanorods, nanoflowers and nanoflakes constitute an interesting research area in various technological applications mainly in nano-electronic devices, energy storage, nanosensing, etc. [1–3]. This is associated with their nanosize dependent novel physico-chemical properties, enhancing their effective surface area and consequently maximizing their reactivity.

Recently, nickel hydroxides and oxides have attracted great attention due to their potential applications in thin-film batteries, electrochromic films, optical materials, fuel cell electrodes, bio-sensing, photocatalysts and electrochemical supercapacitors. Also, nickel hydroxide "$Ni(OH)_2$" has shown an excellent electrochemical properties these last years, including high power density, excellent cyclability and high specific energy; which make it good candidate for many applications specially in batteries [4, 5] and supercapacitors [6, 7]. Indeed, there is two polymorph Ni-Hydroxides: α- and β-$Ni(OH)_2$, with an hexagonal

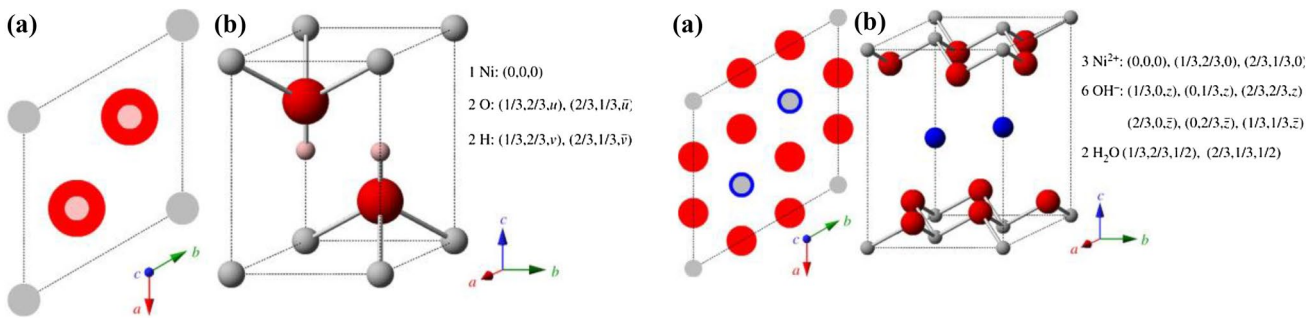

Fig. 1 (Left) The β-$Ni(OH)_2$ crystal structure represented by **a** unit cell projection and **b** ball-and-stick unit cell. (Right) the α-$Ni(OH)_2{\cdot}xH_2O$ ideal crystal structure represented by **a** unit cell projection and **b** ball-and-stick unit cell [11]

layered structures as shown in Fig. 1 [8, 9]. Even though, the α-phase presents higher theoretical electrochemical capacity, it is a metastable turbostratic phase that rapidly changes to the β-phase during the synthesis or in strong alkali media. Therefore, the β-phase is a better candidate for electrochemical material due to their chemical and thermal stability. β-$Ni(OH)_2$ is usually oxidized to β-NiOOH in a charge process and has a maximum theoretical specific capacity of 289 mAh g^{-1} [10].

Some previous works reported the remarkably high specific capacitances of $Ni(OH)_2$ as electrodes in supercapacitors, for instance, N. Parveen and M.H. Cho synthesized 3D flower-like β-$Ni(OH)_2$ with specific capacitance of ~ 1567 F g^{-1} at a current density of 1 A g^{-1} with a solvothermal method based on "bottom up" approach chemistry [12]. Also, N. Naveen and C. Park have fabricated β-$Ni(OH)_2$ nanoplatelets via dendrimer assisted growth on graphene using hydrothermal method with specific capacitance of 2043 F g^{-1} at 5 mV s^{-1} [13]. Moreover, Y. Zhu and C. Cao have obtained α-$Ni(OH)_2$ nanosheets via microwave-assisted liquid-phase growth under low-temperature atmospheric conditions with a specific capacitance of 4172.5 F g^{-1} at 1 A g^{-1} current density [14].

In this framework, we present in this investigation, the synthesis of nickel hydroxides $Ni(OH)_2$ using simple and low-cost free template hydrothermal method at two different growth temperatures with and without SDS surfactant. After that, we have systematically studied the effect of activated carbon (AC, 800 m^2 g^{-1}) addition to these β-Ni $(OH)_2$ products on their mixing electrochemical performance through cyclic voltametric (CV), Galvanostatic charge–discharge (GCD) and electrochemical impedance spectroscopy (EIS) tests.

2 Experimental procedure

2.1 Synthesis of $Ni(OH)_2$ electroactive nanoparticles "NPs"

In a typical synthesis of Ni hydroxide NPs "β-Ni $(OH)_2$", 3 mM of $NiCl_2{\cdot}6H_2O$ was dissolved in distilled water and 10 ml of NaOH aqueous solution was added in the solution. Then, 6 mM of Sodium dodecyl sulfate (SDS) surfactant was added in the final solution which was stirred after that for 1 h. The obtained green solution was then sealed into a 40 mL Teflon-lined stainless steel autoclave and placed in a preheated oven at two different growth temperatures (100 and 160 °C) during 24 h. Next, the fine green gel was filtered washed with distilled water and ethanol for several times to reach neutral pH. Finally, the collected powder was dried at 80 °C for all the night.

2.2 Working electrode preparation

The synthesized β-$Ni(OH)_2$ NPs deposited on Nickel foam (serving as a current collector with areal density of 420 g m^{-2} as well as diameter and thickness of 1.6 mm and 0.2 mm, respectively) "NiF/$Ni(OH)_2$" were prepared by mixing these obtained hydroxide based electroactive products with carbon black "CB" and/or activated carbon "AC" (porous carbon with 800 m^2 g^{-1} specific surface area) (5 wt% CB and 5 wt% AC, or just 10 wt% CB) and polyvinylidene difluride (PVdF) as a binder in a weight ratio of 80:10:10. Nickel foam was covered by this mixture over 1 cm^2 working electrode area which was dried at 60 °C during all the night. According to synthesis condition and electrode preparation, each sample was named as follow:

$\mathbf{NiOH-1}$(160 °C/24 h/ + SDS without AC)
and $\mathbf{NiOH-1/AC}$(160 °C/24 h/ + SDS with AC)

$\mathbf{NiOH-2}$(160 °C/24 h without AC)
and $\mathbf{NiOH-2/AC}$(160 °C/24 h with AC)

$\mathbf{NiOH-3}$(100 °C/24 h without AC)
and $\mathbf{NiOH-3/AC}$(100 °C/24 h with AC)

2.3 Characterization techniques

The product structure were firstly characterized by powder X-ray diffraction (XRD) using an X' Pert PRO diffractometer (PANalytical BV, Netherlands) with theta/2theta geometry, operating with $Cu\text{-}_{K\alpha}$. The mean crystallite size was calculated through the Debye–Scherer equation:

$$D = \frac{K\lambda}{\beta \cos\theta} \quad (1)$$

Where D is the mean crystallite size of the obtained product; λ is the wavelength of $Cu_{k\alpha}$ (1.54056 Å); β is the full width at half-maximum (FWHM) of the intense peak; θ is the Bragg's diffraction angle and K is a constant usually equal to 0.9 [15].

The products morphology has been analyzed by Field Emission Scanning Electron Microscopy (FESEM) using Zeiss Ultra Plus 55 operating at 2 kV. For the FESEM analysis, the products were fixed directly on the sample holder by a graphite paste and prior to all analyses the samples were covered by a thin layer of carbon in order to avoid any problems of charge effect.

The Raman measurements were performed using a JobinYvon Horiba TX 6400 micro-Raman spectrometer equipped with a triple monochromator system to eliminate contributions from Rayleigh lines. All the samples were excited with the 514 nm line of an argon laser with a power of 1.5 mW.

Electrochemical measurements were performed using a Gamry instrument (Reference 600™ Potentiostat/Galvanostat/ZRA) with a three-electrode experimental cell in

6 M KOH aqueous electrolyte. Hg/HgO and Pt electrodes were used as the reference and the counter electrodes, respectively. Cyclic voltammetry (CV) and galvanostatic charge discharge (GCD) experiments of these mixed products were carried out in the positive potential range from 0.6 V to0 V (vs. Hg/HgO), at different scan rate from 1 to 100 mV s^{-1} and at different current density from 1 to 100 A g^{-1}, respectively. Electrochemical impedance spectroscopy (EIS) was performed in the frequency range of 0.1 Hz–100 kHz at an open circuit.

The specific capacitance (C_s) and capacity (Q_s) is usually calculated from CV and CD curves, respectively, according to the following equations [16]:

$$C_s\left(\mathrm{F}\cdot\mathrm{g}^{-1}\right)=\frac{1}{mv\Delta V}\int IdV=\frac{Q}{m\Delta V}\quad \text{from (CV tests)} \tag{2}$$

$$Q_s\left(\mathrm{mAh}\cdot\mathrm{g}^{-1}\right)=\frac{I\Delta t}{3.6m}\quad \text{from (CD tests)} \tag{3}$$

where IdV (mA V), indicates the integrated area under the CV curve, v is the scan rate (mV s^{-1}), ΔV (V) indicates the voltage window, I (A) is the current, Δt (s) is the discharge time, m (g) represents the mass loading of electroactive material.

3 Results and discussion

3.1 Structural and morphological properties of Ni hydroxide based electroactive products

Figure 2 shows the XRD patterns of the as prepared samples under different hydrothermal conditions. These patterns clearly show the formation of selective β-$Ni(OH)_2$ phase according to the JCPDS Card [No 14-0117]. A few distinguishing features of these XRD patterns are for the corresponding peaks to all reflections found with sample (NiOH-3); which are considerably broadened compared to those in samples (NiOH-1) and (NiOH-2), indicating the poor crystallinity of the product which has crystalline badly «bc» form and hence named as β_{bc}–$Ni(OH)_2$ [17–19]. The mean crystallite size calculated according to Eq. (1) is found to be around 18 nm, 20 nm and 6 nm for the samples (NiOH-1), (NiOH-2), (NiOH-3) respectively, confirming thus the formation of the nanocrystalline structure. The broaded peaks found with NiOH-3 confirm the obtained low crystallite size of particles.

Table 1 compares the mean crystallite size of the obtained $Ni(OH)_2$-NPs with others from the literature. From this table, we can clearly see that our results obtained by hydrothermal method with the optimized parameters show the lower mean crystallite size in the range 6–20 nm in comparison with the literature.

Figure 3 illustrates Raman spectra of these obtained Ni based hydroxides which confirm the β-$Ni(OH)_2$ and

Table 1 Mean crystallite size of $Ni(OH)_2$-NPs synthesized with different process and at different conditions (evaluated from the Debye–Scherer equation)

Synthesis procedure [References]	Crystallite size (nm)
Precipitation [19]	36.5
Electrodialysis [20]	35
Hydrothermal [21]	45.8
Our condition (hydrothermal)	**6–20**

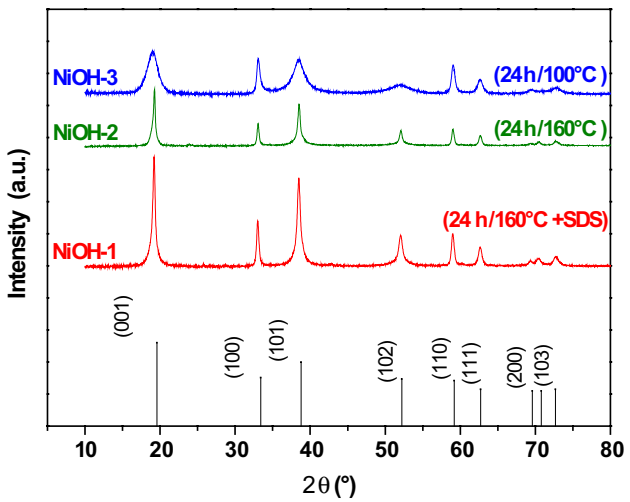

Fig. 2 XRD patterns of the β-$Ni(OH)_2$ hydroxides synthesized in different hydrothermal conditions

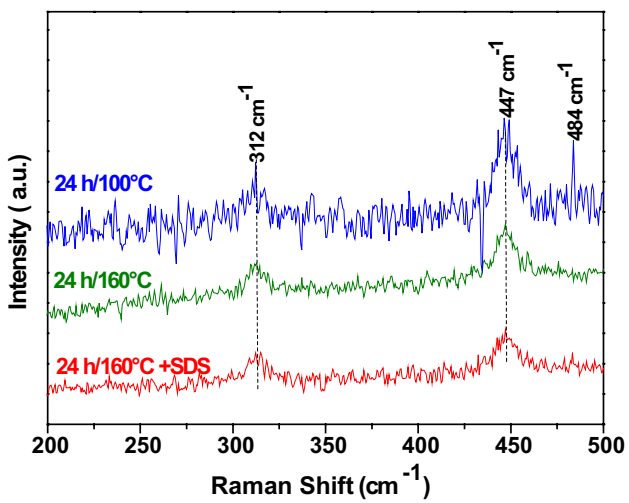

Fig. 3 Raman spectra of the obtained β-phase $Ni(OH)_2$ hydroxide using hydrothermal method at different conditions

β_{bc}-$Ni(OH)_2$ structural phase formation according to the literature [20, 22]. So, the obtained peaks at 312 and 447 cm^{-1} can be ascribed to the E-type vibration of the Ni–OH lattice and the Ni-O stretch, respectively. An additional peak around 484 cm^{-1} is observed just for NiOH-3 sample and can be ascribed to Ni–O stretching vibration of Ni^{+2} species associated with O^{-2} for β_{bc}-$Ni(OH)_2$ phase which is consistent with the XRD results.

Morphological characteristics of these Ni based hydroxide products were investigated by FESEM microscopy, as shown in Fig. 4. The observed morphology is spherical-like NPs in agglomerate nanoclusters. The nanoparticle size distributions found by measuring maximum diameters of more than 100 NPs are also shown in the right of the corresponding FESEM micrographs.

The average nanoparticles size was found to be around 22 nm, 27 nm, 8 nm for (a), (b) and (c), respectively. We can clearly see that the addition of SDS as a surfactant and the growth temperature played a significant role in decreasing hydroxide NPs diameter.

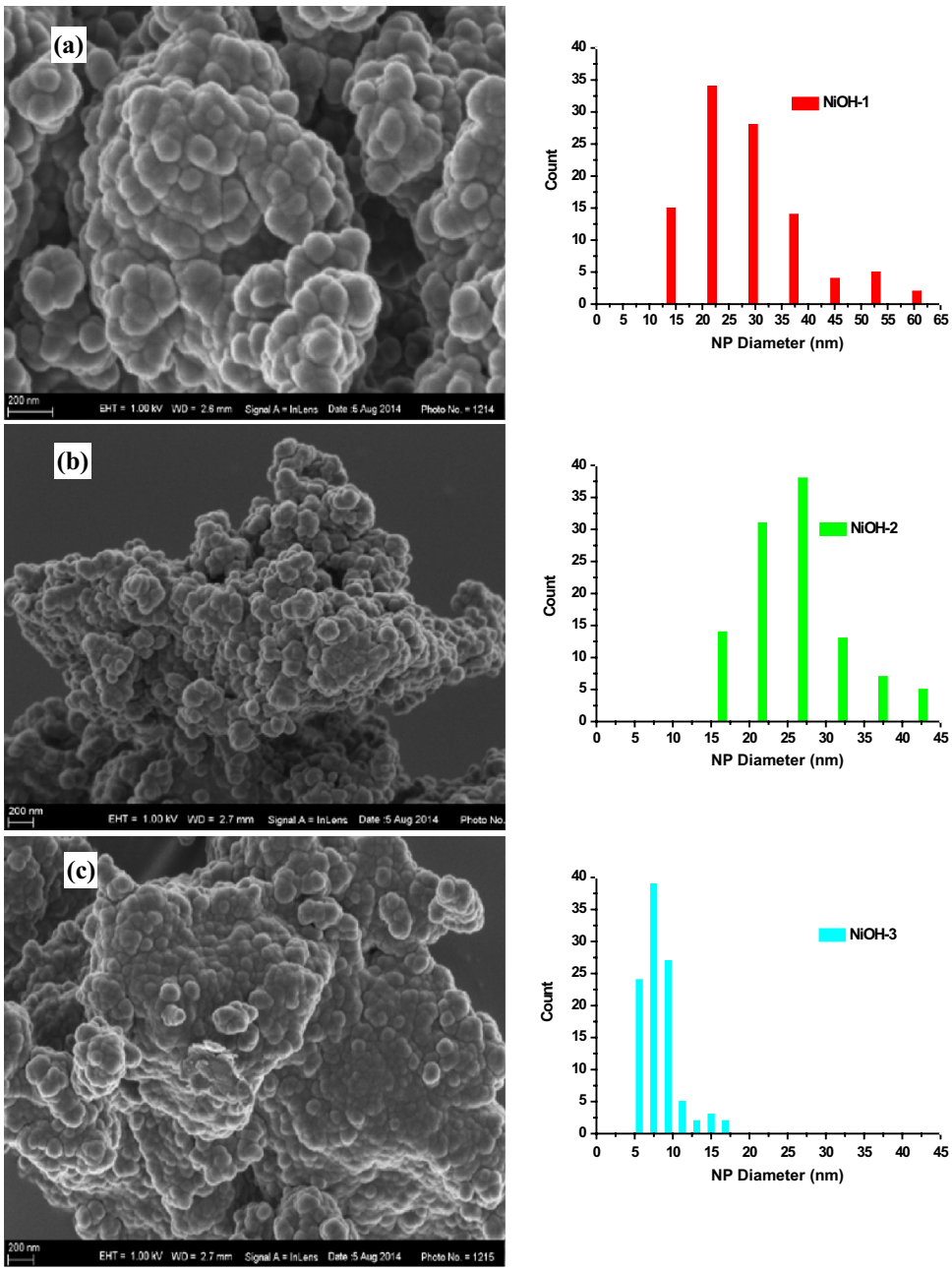

Fig. 4 FE-SEM micrographs of β-$Ni(OH)_2$ hydroxides synthesized at different hydrothermal conditions: **a** 160 °C/24 hwith SDS "Ni(OH)-1", **b** 160 °C/24 h "Ni(OH)-2" and **c** 100 °C/24 h "Ni(OH)-3"

3.2 Electrochemical measurements

3.2.1 Cyclic voltammetry results

Cyclic voltammetry (CV) test is considered as a suitable tool to indicate the capacitive behavior of an electroactive material. Figure 5 shows the obtained CV curves of the synthesized β-$Ni(OH)_2$ at different experimental conditions with and without AC in 6 M KOH electrolyte at different scan rate from 1 to 100 mV s^{-1} at the positive potential range from 0 to 0.6 V (vs. Hg/HgO reference electrode). The shape of these CV curves indicates clearly the faradic or redox behavior different from the electric double layer capacitance (EDLC) behavior in which the shape is normally close to an ideal rectangular shape [23–25]. We can observe in all CV curves the redox pair peaks around 0.3 V and 0.5 V, corresponding to the following electrochemical reaction which confirms a pseudocapacitive mechanism according to the Ref. [26]:

$$\beta - Ni(OH)_2 + (OH)^- \Leftrightarrow \beta - NiOOH + H_2O + e^-$$

The anodic and cathodic peaks potential shift to more positive and negative positions, respectively. It should be noted also that the current increases with increasing the scan rate and the CV curves shape change accordingly.

More precisely, Fig. 6a, b display the CV curves of these mixed electroactive materials (with and without AC) at 5 mV s^{-1} scan rate where we can clearly see their effect on the resultant current. Note that the CVs of mixed β-$Ni(OH)_2$/AC electrodes have higher current response and larger surface area than those of the pure hydroxide, which suggests that the specific capacitance of electroactive materials is higher. Also, a linear relationship is observed (Fig. 6d) between the peak current and the scan rate square root which demonstrates that this redox faradic reaction is controlled by proton diffusion [27, 28]. The enhanced performance of $NiOH_2$/AC can be attributed to the improved electrical conductivity, facilitated ion

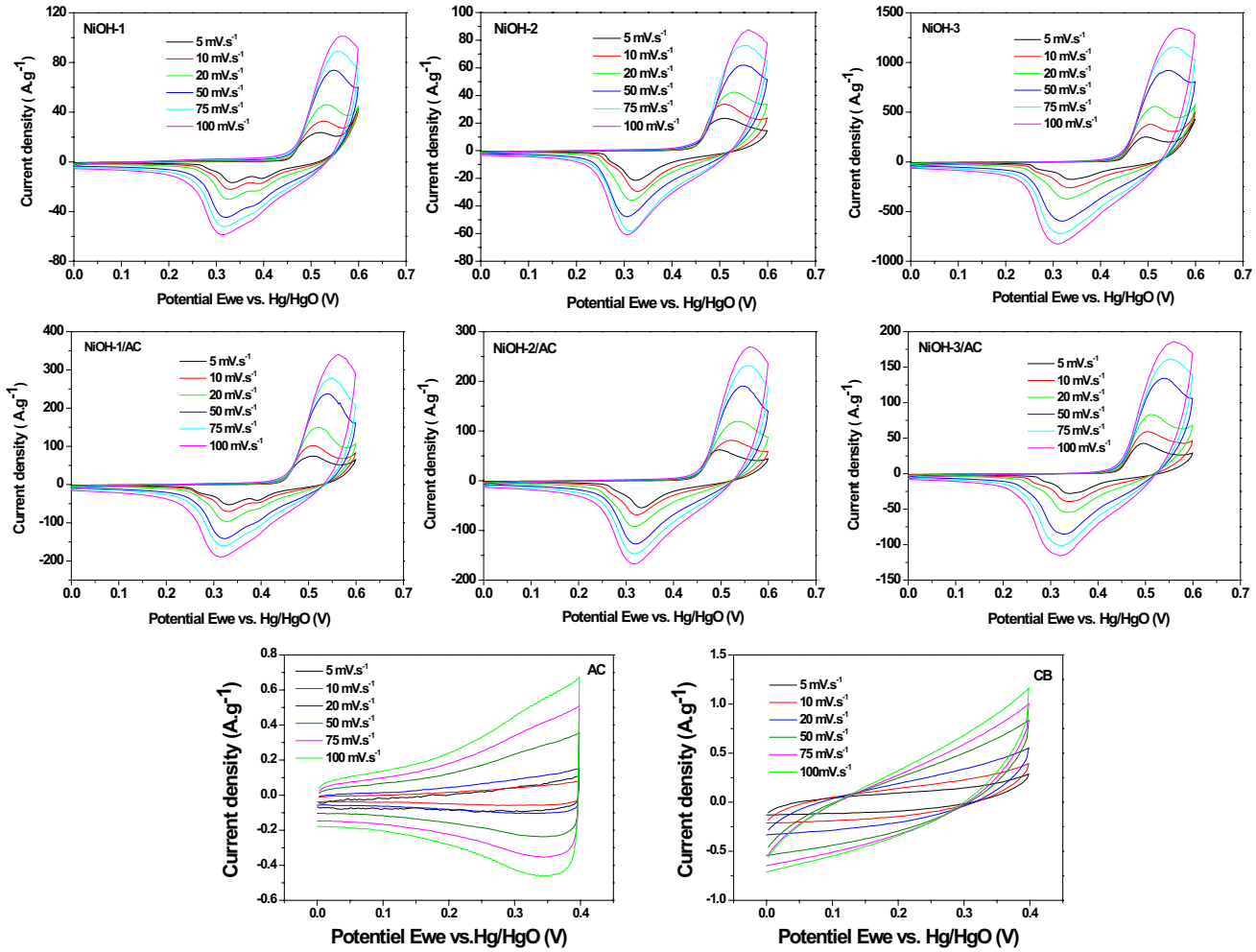

Fig. 5 Cyclic voltammograms of hydroxide samples at different scan rate

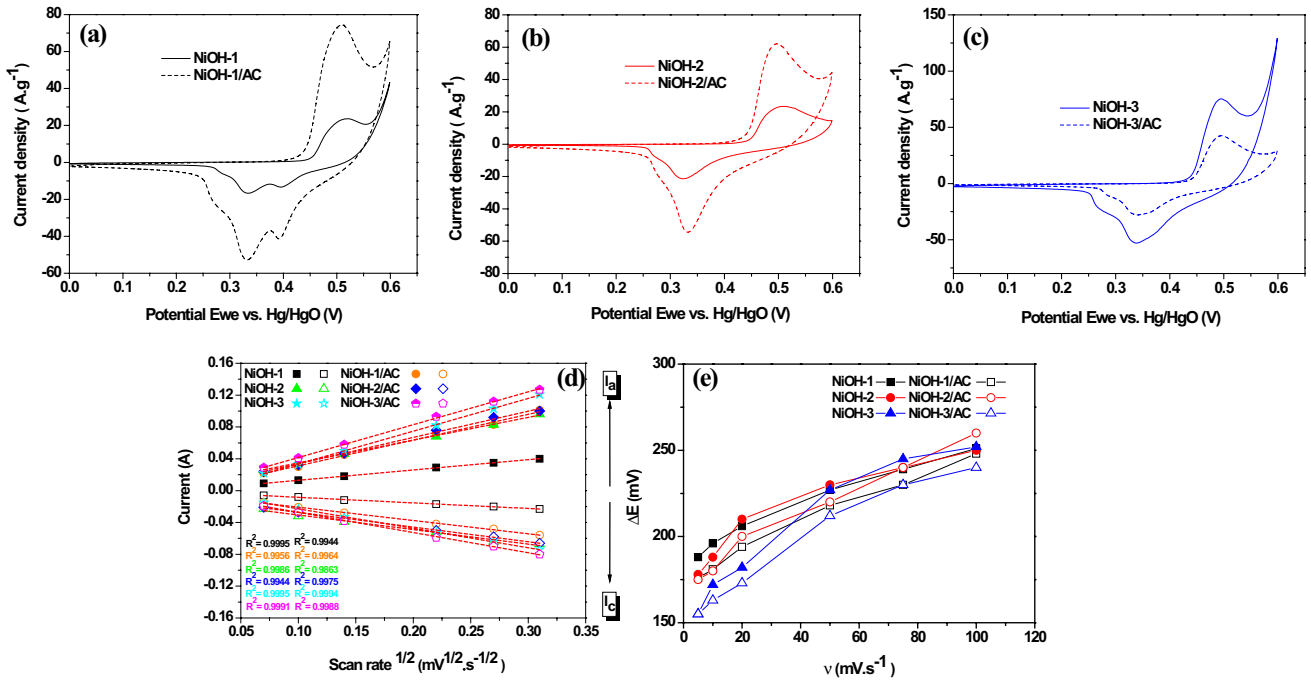

Fig. 6 Electrochemical properties of β-Ni(OH)$_2$ NPs electrodes: **a**–**c** CV curves at 5 mV s^{-1} with and without AC and relationship between i_p and $v^{1/2}$ (**d**) and potential difference ΔE in function of scan rate (**e**)

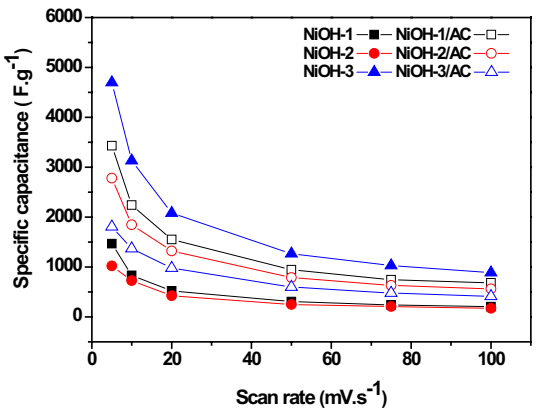

Fig. 7 Specific capacitance at different scan rate

transport and diffusion rate [29]. However, the potential difference ($\Delta E = E_{Oxy} - E_{Red}$) is taken as a measure of the redox reaction reversibility; smaller value, more reversibility. Figure 6d shows the dependence of the ΔE values on the sweep rate. These values are significantly increasing for electrode NiOH-1, NiOH-1/AC, NiOH-2 and NiOH-2/AC at faster scan rates, unlike NiOH-3 and NiOH-3/AC based electrodes. Therefore, products with least ΔE (< 200 mV) are more reversible than the others; this is in accordance with Ref. [30, 31].

The specific capacitance of these products was calculated using (Eq. 2) and represented in Fig. 7. We confirm, as already reported in the literature, that the capacitance decreases with the increase of scan rate. This decrease may be explained by referring to the diffusion effect, that is to say, the inner active sites in the electrode are inaccessible at high scan rates [32, 33]. In the case of NiOH-3, the product has the highest specific capacitance value about 4697 F g^{-1} at 5 mV s^{-1}. Consequently, this is due to the fact that the electrochemical performances of β_{bc}-nickel hydroxide are higher than that of β-nickel hydroxide [19–34]. These values are higher than those obtained in literature for other hydroxide nanocomposites [14, 16, 33, 35–40] (as summarized in Table 2).

Moreover, the presence of nickel hydroxide can produce the Faradaic pseudo-capacitance; at the same time, activated carbon with his high specific area can provide both a large double layer capacitance and an excellent conductivity, thus the specific capacitance of this electroactive material, as combination of double-layer capacitance and Faradaic pseudocapacitance, can be promoted greatly more with NiOH-1 and -2 [41].

3.2.2 Galvanostatic charge–discharge results

To better understand the electrochemical properties of these produced hydroxides, the charge–discharge behavior was performed, as shown in Fig. 8a. These obtained curves are similar and show a significant deviation from a straight and flat line, indicating that the capacity mainly

Table 2 Specific capacitance of some Ni hydroxide depending to the synthesis method, electrolyte and position of our results

Electroactive material	Synthesis method	Electrolyte	Cs (F g^{-1})	References
β-$Ni(OH)_2$	Exfoliation-free sol–gel route	6 M KOH	1735 (5 mV s^{-1})	[35]
α-$Ni(OH)_2$	Microwave-assisted method	6 M KOH	4172.5 (1 A g^{-1})	[14]
α-$Ni(OH)_2$	Electrodeposition	1 M KOH	2424 (2 mV s^{-1})	[16]
MWCNT/amor-$Ni(OH)_2$	Coordinating etching and precipitating	1 M KOH	1540 (5 mV s^{-1})	[36]
β-$Ni(OH)_2$	Hydrothermal	2 M KOH	1295 (5 mV s^{-1})	[33]
$Ni(OH)_2$/GN	Plasma-enhanced CVD	1 M KOH	1667(5 mV s^{-1})	[37]
α-$Ni(OH)_2$/G	Microwave-assisted method	6 M KOH	1735(1 mV s^{-1})	[38]
$Ni(OH)_2$/GN	In situ crystallization	6 M KOH	1444(5 mV s^{-1})	[39]
$Ni(OH)_2$/rGO/NF	Oxidization and exfoliation	6 M KOH	1433(5 mV s^{-1})	[40]
β-$Ni(OH)_2$	Hydrothermal	6 M KOH	4697 (5 mV s^{-1})	Our work
β-$Ni(OH)_2$/AC			3431(5 mV s^{-1})	

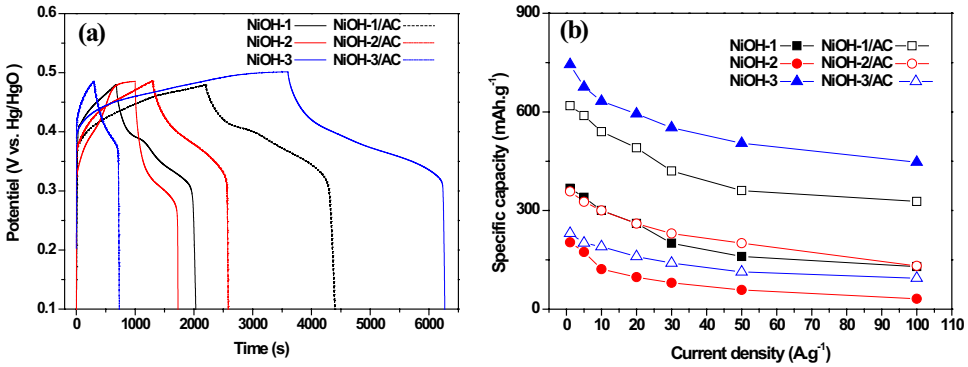

Fig. 8 **a** Galvanostatic charge–discharge curves at 1 A g^{-1}, **b** specific capacity as a function of the scan rate for β-$Ni(OH)_2$ products with and without AC

comes from the Faradaic redox reactions confirming the previous results. The discharge specific capacity of the obtained samples at different current density ranging from 1 to 100 A g^{-1} were calculated using (Eq. 3) and depicted in Fig. 8b. Evidently, it presents already a diminution in values as a function with current density also we can say that the AC plays an important role.

The electrochemical charge storage capacity of nickel hydroxide is strongly correlated to the extent of structural disorder where crystalline samples exhibit poor electrochemical activity.

At a fixed discharge current density, the longer the discharge time is, the greater the corresponding specific capacity [32]. As shown in Fig. 8a, the NiOH-3 and NiOH-2/AC based electrodes exhibits the highest specific capacity which is consistent with the CV result, suggesting the remarkably improved electrochemical performance of this pure and mixed material.

3.2.3 Electrochemical impedance spectroscopy results

To extensively characterize the electrochemical properties of these synthesized hydroxides and their mixing with AC, electrochemical impedance spectroscopy "EIS" over the frequency range of 0.1 to 100 kHz in 6 M KOH solution was measured in an open circuit potential (E_{oc}). Figure 9 shows their Nyquist plots with similar shape; they display a linear part in the low-frequency region and a small semi-circle in the high-frequency region.

The Nyquist plots are fitted to their specific electronic circuit model as shown in the figure; where R_s stands for the equivalent series resistance related to the ionic resistance of the electrolyte: the intrinsic resistance of the substrate and the contact resistance at the active material/current collector interface (equivalent to high frequency intercept on the real Z or x axis); L is the self-inductance related to electrical connections [42]; W is a Warburg impedance arising from a diffusion-controlled process at low frequency; R_{ct} is the charge transfer resistance of the double-layer capacitance [43] and the constant phase element (CPE, Q) was used to replace the double-layer capacitance (Cdl) because of the deviation from an ideal capacitor [44]. Moreover, the straight line found with angle lower than 45° for all samples is the capacitative behavior characteristic under diffusion control. However, the difference in straight lines slopes represents the diffusive resistance [42].

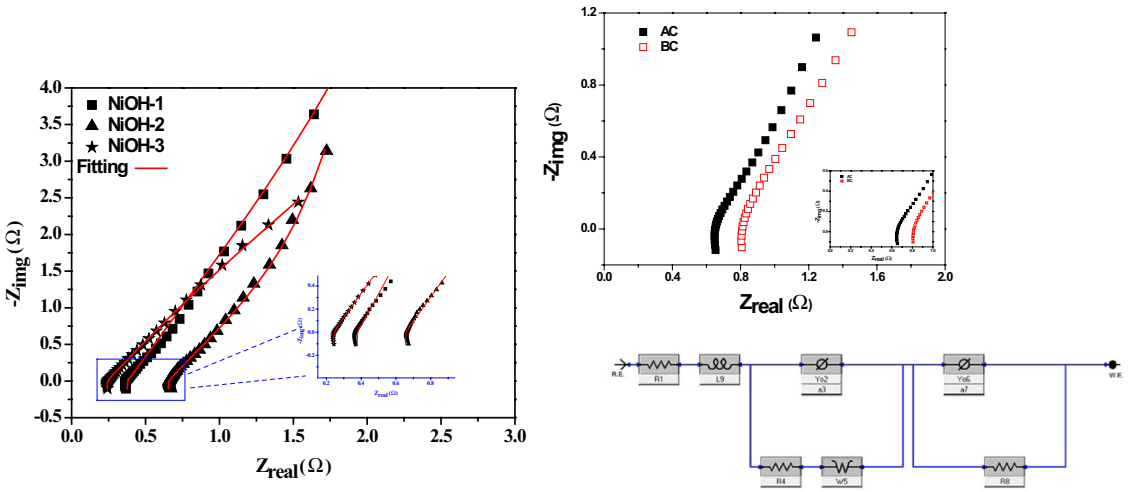

Fig. 9 Nyquist plots of β-Ni(OH)$_2$ NPs based electrodes with and without AC, (right) equivalent fitting circuit and impedance at high frequency region

Based on this simulation, the calculated values for equivalent series resistance and charge transfer resistance are shown in Table 3. It is found that the mixing based of β-Ni(OH)$_2$ and AC display smallest R_s and R_{ct} values than that pure one without AC; which is consistent with the CV and CD results indicating the lower electrode intrinsic resistance with better ability of storing charges. Also, we can say that these values are smaller than those mentioned in the literature [45, 46]. The low transfer resistances indicated that our simple strategy of AC addition could effectively enhance the conductivity and facilitate the redox reactions at the electrode/electrolyte interface.

3.2.4 Electroactive mass loading effect

To investigate the effect of electroactive mass on the electrochemical performance of our products; EC measurements have been carried out with different loading mass and were compared with previous results (NiOH-1, NiOH-3 and NiOH-3/AC). The new electrodes were labeled by mass: 3.3 mg NiOH-1, 7 mg NiOH-3, 1.2 mg NiOH-3/AC. Their CVs also showed the characteristic peaks assigned to Faradic reactions (Fig. 10a–c). We can see clearly that the current decreases with increasing the Ni(OH)$_2$ mass, consistent with the diminution of discharge duration (see Fig. 10d–f) and slightly increase in the internal resistance as shown in Fig. 10g–i.

The specific capacitance of these electrodes at different scan rates were calculated according to the Eq. (2) and illustrated in Fig. 10g–i. The specific capacitance found with 3.3 mg NiOH-1, 7 mg NiOH-3 and 1.2 mg NiOH-3/AC at 5 mV s^{-1} are 546 F g^{-1}, 84 F g^{-1} and 1220 F g^{-1} while it's up to 1467 F g^{-1}, 4697 F g^{-1} and 1807 F g^{-1} for NiOH-1, NiOH-3 and NiOH-3/AC, respectively, with 1 mg weight (see Fig. 11).

Moreover, the CD curves confirm that the electroactive product with less loading mass has the longer discharge time, so the highest specific capacity. So, with increasing the loading mass, the capacity decreased and the reason may be due to "more mass, so, large electroactive material thickness and high resistance for a fixed electrode size" [47]. Therefore, it can stated that the additional β-Ni(OH)$_2$ nanoparticles, especially for those located far away from the NiF surface, do not actively participate in pseudocapacitive reactions [48].

3.2.5 Cycling performance

Cycling stability is another important parameter for evaluating the electrochemical performance of our hydroxides for supercapacitor lifetime. Figure 12 displays the discharge specific capacity retention and the Coulombic efficiency for two of our products NiOH-2 and NiOH-3/AC as a function of the cycle number at 30 A g^{-1} constant current density. As shown

Table 3 Equivalent series "R_s" and charge transfer "R_{ct}" resistances of our β-Ni(OH)$_2$ products with and without AC

	NiOH-1	NiOH-1/AC	NiOH-2	NiOH-2/AC	NiOH-3	NiOH-3/AC
R_s (Ω)	0.37	0.28	0.67	0.38	0.24	0.23
R_{ct} (Ω)	0.42	0.37	0.68	0.32	0.49	0.43

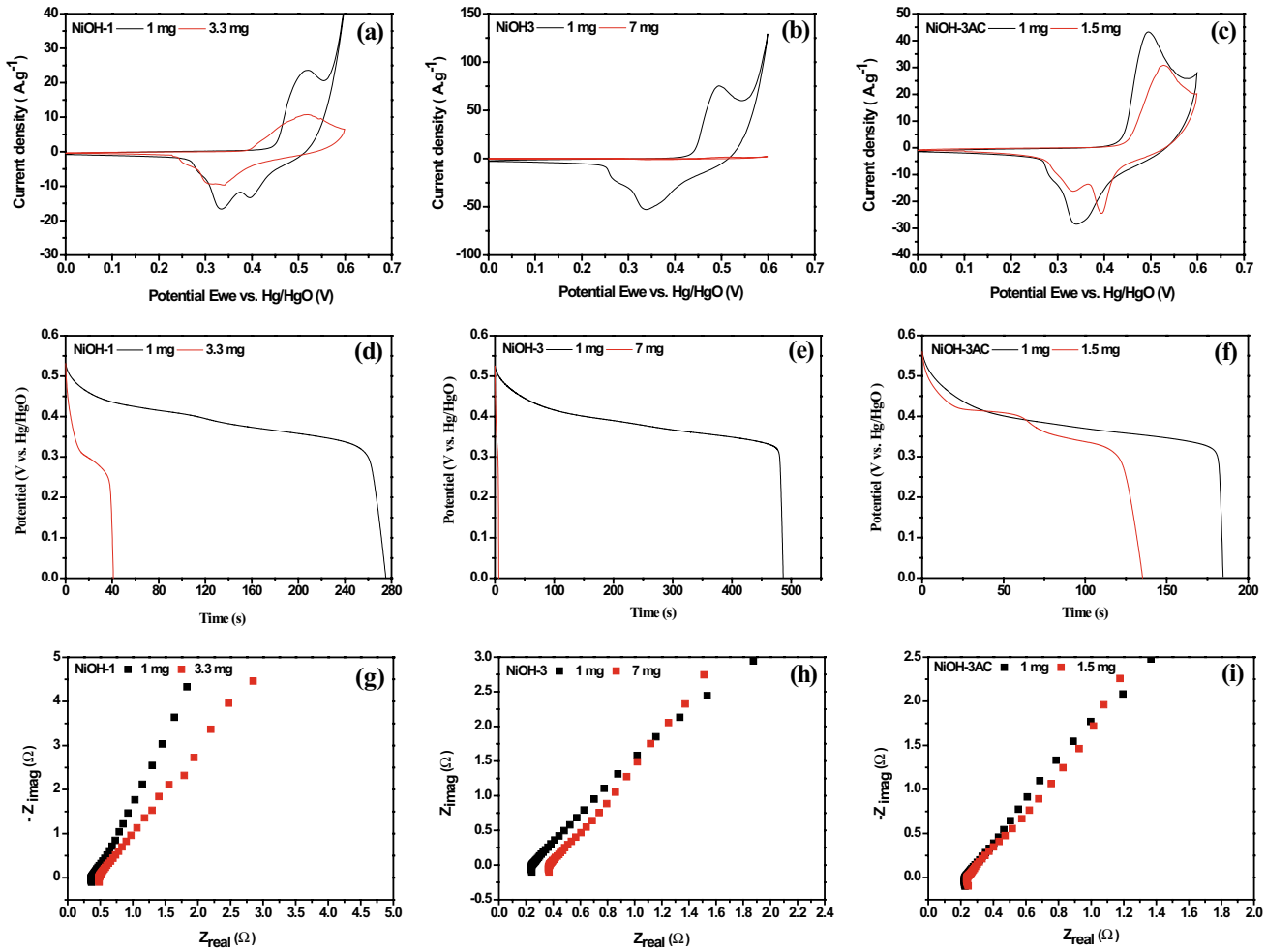

Fig. 10 CV curves at 5 mV s^{-1} scan rate (**a**–**c**), discharge curves at 5 A g^{-1} current density (**d**–**f**), Nyquist plots (**g**–**i**), of these hydroxides with and without AC using different mass loading

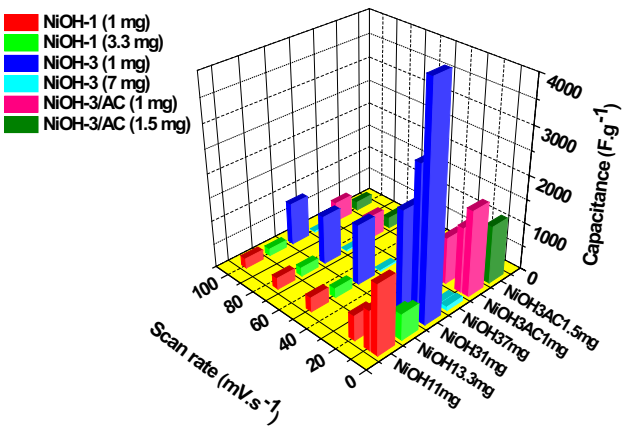

Fig. 11 Specific capacitance for different mass loading electroactive products

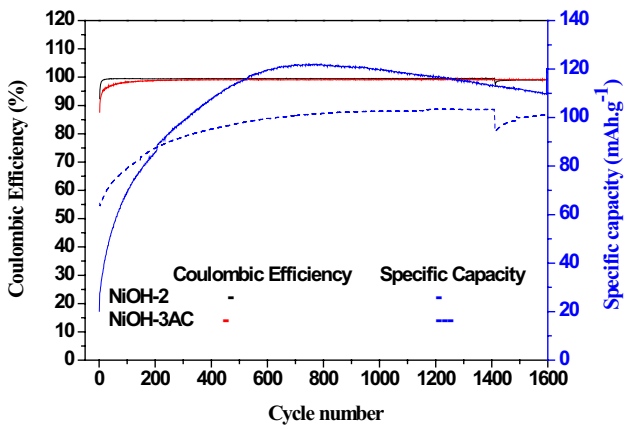

Fig. 12 Cycling performance and Coulombic efficiency over 1700 cycles for NiOH-2 and NiOH-3/AC electroactive materials

in this figure, the specific capacity of these two products initially increases and then becomes almost constant after 600 cycles (slight decrease with number of cycles for NiOH-3/AC). After 1700 cycles, the coulombic efficiency retention is around 99.06% (103 mAh g^{-1}) and 99.05% (109 mAh g^{-1}), for NiOH-2 and NiOH-3/AC, respectively, indicating an excellent long-term stability for this kind of electroactive Ni based hydroxide.

4 Conclusion

The hydroxide spherical agglomerate nanoparticles β-phase $Ni(OH)_2$ and β_{bc}-$Ni(OH)_2$ with a low average size ranging from 8 nm to 27 nm were successfully synthesized via a simple and low cost free template hydrothermal method. The structural study confirmed the obtention of β-$Ni(OH)_2$ pure brucite crystalline phase in spherical nanoparticle morphology. Evidently, the additions of SDS as a surfactant and the growth temperature have played a significant role in decreasing hydroxide NPs diameter. The incorporation of activated carbon (AC) to these nanoparticles (β_{bc}-$Ni(OH)_2$ and β-$Ni(OH)_2$) have shown enhancement in the capacitance of the electroactive material in the second case, the electrolyte–electrode accessibility and their conductivity. The electrochemical properties exhibited a very high specific capacitance (capacity) around 4697 F g^{-1} (744 mAh g^{-1}) and 3431 F g^{-1} (618 mAh g^{-1}) at a scan rate of 5 mV s^1 (or at current density of 1 A g^{-1}), for NiOH-3 and NiOH-1 AC, respectively. Consequently, our results showed that the synthesized materials demonstrated an excellent cycle life with a coulombic efficiency of 99.5% after 1700 cycles at a 30 A g^{-1} current density. These values are higher than those obtained in literature for other hydroxide nanocomposites suggesting their highly promising application in supercapacitors field.

Acknowledgements The present work is based on the research supported by the Algeria and South Africa collaboration program between LEREC laboratory, Badji Mokhtar-Annaba University and South African Research Chairs Initiative (SARChI) in Carbon Technology and Materials of the Department of Science and Technology. The financial support received from National Research Foundation (NRF) from Pretoria and Directorate General for Scientific Research and Technological Development (DGRSDT) from Algeria.

Compliance with ethical standards

Conflict of interest The authors declare that they have no conflict of interest.

References

1. Wu L, Wu Y, Wei H, Shi Y, Hu C (2004) Synthesis and characteristics of NiO nanowire by a solution method. Mater Lett 58:2700–2703. https://doi.org/10.1016/j.matlet.2004.03.047
2. Castro EB, Real SG, Pinheiro Dick LF (2004) Electrochemical characterization of porous nickel–cobalt oxide electrodes. Int J Hydrog Energy 29:255–261. https://doi.org/10.1016/S0360-3199(03)00133-2
3. Aghazadeh M, Golikand AN, Ghaemi M (2011) Synthesis, characterization, and electrochemical properties of ultrafine β-$Ni(OH)_2$ nanoparticles. Int J Hydrog Energy 36:8674–8679. https://doi.org/10.1016/j.ijhydene.2011.03.144
4. Chen J, Bradhurst DH, Dou SX, Liu HK (1999) Nickel hydroxide as an active material for the positive electrode in rechargeable alkaline batteries. J Electrochem Soc 146:3606–3612
5. Yang CC (2002) Synthesis and characterization of active materials of Ni $(OH)_2$ powders. Int J Hydrog Energy 27(10):1071–1081. https://doi.org/10.1016/S0360-3199(02)00013-7
6. Kong X, Liu X, He Y, Zhang D, Wang X, Li Y (2007) Hydrothermal synthesis of β-nickel hydroxide microspheres with flake-like nanostructures and their electrochemical properties. Mater Chem Phys 106(2–3):375–378. https://doi.org/10.1016/j.matchemphys.2007.06.015
7. Wang H, Casalongue HS, Liang Y, Dai H (2010) $Ni(OH)_2$ nanoplates grown on graphene as advanced electrochemical pseudocapacitor materials. J Am Chem Soc 132(21):7472–7477. https://doi.org/10.1021/ja102267j
8. Cabanas-Polo S, Suslick KS, Sanchez-Herencia AJ (2011) Effect of reaction conditions on size and morphology of ultrasonically prepared Ni $(OH)_2$ powders. Ultrason Sonochem 18:901–906. https://doi.org/10.1016/j.ultsonch.2010.11.017
9. Oliva P, Laurent JF, Daney BA, Delmas C, Braconnier JJ, Fievet F, Nosay RD (1982) Review of the structure and the electrochemistry of nickel hydroxides and oxy-hydroxides. J Power Sources 8(2):229–255. https://doi.org/10.1016/0378-7753(82)80057-8
10. Liu HB, Xiang L, Jin Y (2006) Hydrothermal modification and characterization of $Ni(OH)_2$ with high discharge capability. Cryst Growth Des 6(1):283–286. https://doi.org/10.1021/cg050119p
11. Hall DS, Lockwood DJ, Bock C, MacDougall BR (2014) Nickel hydroxides and related materials: a review of their structures, synthesis and properties. Proc R Soc A 471:20140792. https://doi.org/10.1098/rspa.2014.0792
12. Parveen N, Cho MH (2016) Self-assembled 3D flower-like nickel hydroxide nanostructures and their supercapacitor applications. Sci Rep 6:2–11. https://doi.org/10.1038/srep27318
13. Naveen N, Park C, Sohn KS, Pyo M (2017) Nickel hydroxide nanoplatelets via dendrimer-assisted growth on graphene for high-performance energy-storage applications. Electrochim Acta 248:313–321. https://doi.org/10.1016/j.electacta.2017.07.156
14. Zhu Y, Cao C, Tao S, Chu W, Wu Z, Li Y (2014) Ultrathin nickel hydroxide and oxide nanosheets: synthesis, characterizations and excellent supercapacitor performances. Sci Rep 4:1–7. https://doi.org/10.1038/srep05787
15. Theivasanthi T, Kartheeswari N, Alagar M (2013) Chemical precipitation synthesis of ferric chloride doped zinc sulphide nanoparticles and their characterization studies. Chem Sci Trans 2:497–507. https://doi.org/10.7598/cst2013.207
16. Aghazadeh M, Ghaemi M, Sabour B, Dalvand S (2014) Electrochemical preparation of α-$Ni(OH)_2$ ultrafine nanoparticles for high-performance supercapacitors. J Solid State Electrochem 18:1569–1584. https://doi.org/10.1007/s10008-014-2381-7
17. Ramesh TN, Kamath PV (2008) The effect of stacking faults on the electrochemical performance of nickel hydroxide electrodes. Mater Res Bull 43:2827–2832. https://doi.org/10.1016/j.materresbull.2008.06.010
18. Faure C, Delmas C (1991) Characterization of a turbostratic α-nickel hydroxide quantitatively obtained from an $NiSO_4$ solution. J Power Sources 35(3):279–290. https://doi.org/10.1016/0378-7753(91)80112-B

19. Jayashree RS, Kamath PV, Subbanna GN (2000) The effect of crystallinity on the reversible discharge capacity of nickel hydroxide. J Electrochem Soc 147(6):2029–2032. https://doi.org/10.1149/1.1393480
20. Narayan RT (2015) Effect of crystallinity of β- and βbc-nickel hydroxide samples on chemical cycling. Ind J Mater Sci 2015:1–7. https://doi.org/10.1155/2015/820193
21. Deabate S, Fourgeot F, Henn F (2000) X-ray diffraction and micro-raman spectroscopy analysis of new nickel hydroxide obtained by electrodialysis. J Power Sources 87(1–2):125–136. https://doi.org/10.1016/S0378-7753(99)00437-1
22. Ramesh TN, Kamath PV (2009) The effect of crystallinity and structural disorder on the electrochemical performance of substituted nickel hydroxide electrodes. J Solid State Electrochem 13:763–771. https://doi.org/10.1007/s10008-008-0591-6
23. Qu R, Dai Z, Zhu Z, Haarberg GM (2017) Facile preparation of layered $Ni(OH)_2$/graphene composite from expanded graphite. Int J Electrochem Sci 12:8833–8846. https://doi.org/10.20964/2017.10.72
24. Qu R, Tang S, Qin X, Yuan J, Deng Y, Wu L, Wei Z (2017) Expanded graphite supported $Ni(OH)_2$ composites for high performance supercapacitors. J Alloys Compd 728:222–230. https://doi.org/10.1016/j.jallcom.2017.08.270
25. Ji Y, Liu W, Zhang Z, Wang Y, Zhao X, Li B, Wang X, Liu X, Liu B, Fenga S (2017) Heterostructural MnO_2@NiS_2/$Ni(OH)_2$ materials for high-performance pseudocapacitor electrodes. RSC Adv 7:44289–44295. https://doi.org/10.1039/c7ra06569h
26. Xu S, Li X, Yang Z, Wang T, Jiang W, Yang C, Wang S, Hu N, Wei H, Zhang Y (2016) Nanofoaming to boost the electrochemical performance of Ni@$Ni(OH)_2$ nanowires for ultrahigh volumetric. ACS Appl Mater Interfaces 8:27868–27876. https://doi.org/10.1021/acsami.6b10700
27. Li L, Xu J, Lei J, Zhang J, Mclarnon F, Wei Z, Pan F (2015) A one-step, cost-effective green method to in situ fabricate $Ni(OH)_2$ hexagonal platelets on Ni foam as binder-free supercapacitor electrode materials. J Mater Chem A 3:1953–1960. https://doi.org/10.1039/c4ta05156d
28. Lv S, Suo H, Wang J, Wang Y, Zhao C, Xing S (2012) Facile synthesis of nanostructured $Ni(OH)_2$ on nickel foam and its electrochemical property. Colloids Surf A Physicochem Eng Asp 396:292–298. https://doi.org/10.1016/j.colsurfa.2012.01.011
29. Tessier C, Haumesser PH, Bernard P, Delmas C (1999) The structure of $Ni(OH)_2$: from the ideal material to the electrochemically active one. J Electrochem Soc 146(6):2059–2067. https://doi.org/10.1149/1.1391892
30. Huang Q, Wang X, Li J, Dai C, Gamboa S, Sebastian PJ (2007) Nickel hydroxide/activated carbon composite electrodes for electrochemical capacitors. J Power Sources 164:425–429. https://doi.org/10.1016/j.jpowsour.2006.09.066
31. Laviron E (1979) General expression of the linear potential sweep voltammogram in the case of diffusion less electrochemical systems. J Electroanal Chem 101(1):19–28. https://doi.org/10.1016/S0022-0728(79)80075-3
32. Cai FS, Zhang GY, Chen J, Gou XL, Liu HK, Dou SX (2004) $Ni(OH)_2$ tubes with mesoscale dimensions as positive-electrode materials of alkaline rechargeable batteries. Angew Chem Int Ed 43:4212–4216. https://doi.org/10.1002/anie.200460053
33. Sarac FE, Unal U (2015) Electrochemical-hydrothermal synthesis of manganese oxide films as electrodes for electrochemical capacitors. Electrochim Acta 178:199–208. https://doi.org/10.1016/j.electacta.2015.07.169
34. Ma X, Li Y, Wen Z, Gao F, Liang C, Che R (2015) Ultrathin β-$Ni(OH)_2$ nanoplates vertically grown on nickel-coated carbon nanotubes as high-performance pseudocapacitor electrode materials. ACS Appl Mater Interfaces 7:974–979. https://doi.org/10.1021/am5077183
35. Cui H, Xue J, Ren W, Wang M (2014) Ultra-high specific capacitance of β-$Ni(OH)_2$ monolayer nanosheets synthesized by an exfoliation-free sol–gel route. J Nanopart Res 16:2601. https://doi.org/10.1007/s11051-014-2601-1
36. Jiang W, Yu D, Zhang Q, Goh K, Wei L, Yong Y (2015) Ternary hybrids of amorphous nickel hydroxide–carbon nanotube-conducting polymer for supercapacitors with high energy density, excellent rate capability, and long cycle life. Adv Funct Mater 2015:1–11. https://doi.org/10.1002/adfm.201403354
37. Wang X, Wang Y, Zhao C, Zhao Y, Yan B (2012) Electrodeposited $Ni(OH)_2$ nanoflakes on graphite nanosheets prepared by plasma-enhanced chemical vapor deposition for supercapacitor electrode. New J Chem 36:1902–1906. https://doi.org/10.1039/C2NJ40308K
38. Yan J, Fan Z, Sun W, Ning G, Wei T, Zhang Q (2012) Advanced asymmetric supercapacitors based on $Ni(OH)_2$/graphene and porous graphene electrodes with high energy density. Adv Funct Mater 2012:1–10. https://doi.org/10.1002/adfm.201102839
39. Yan H, Bai J, Wang J, Zhang X, Wang B, Liu Q, Liu L (2013) Graphene homogeneously anchored with $Ni(OH)_2$ nanoparticles as advanced supercapacitor electrodes. RSC 15:10007–10015. https://doi.org/10.1039/c3ce41361f
40. Zhang C, Chen Q, Zhan H (2016) Supercapacitors based on reduced graphene oxide nanofibers supported $Ni(OH)_2$ nanoplates with enhanced electrochemical performance. ACS Appl Mater Interfaces 8:22977–22987. https://doi.org/10.1021/acsami.6b05255
41. Shruthi B, Madhu BJ, Raju VB, Vynatheya S, Devi BV, Jayashree GV, Ravikumar CR (2017) Synthesis, spectroscopic analysis and electrochemical performance of modified β-nickel hydroxide electrode with CuO. J Sci Adv Mater Dev 2:93–98. https://doi.org/10.1016/j.jsamd.2016.12.002
42. Bello A, Fashedemi OO, Momodu DY, Barzegar F, Masikhwa TM, Madito MJ, Manyala N (2015) Electrochemical studies of microwave synthesized bimetallic sulfides nanostructures as faradaic electrodes. Electrochim Acta 174:778–786. https://doi.org/10.1016/j.electacta.2015.06.072
43. Wu Z, Huang XL, Wang ZL, Xu JJ, Wang HG, Zhang XB (2014) Electrostatic induced stretch growth of homogeneous β-$Ni(OH)_2$ on graphene with enhanced high-rate cycling for supercapacitors. Sci Rep 4:1–8. https://doi.org/10.1038/srep03669
44. Li X, Ding R, Shi W, Xu Q, Ying D, Huang Y, Liu E (2018) Hierarchical porous Co(OH)F/$Ni(OH)_2$: a new hybrid for supercapacitors. Electrochim Acta 265:455–473. https://doi.org/10.1016/j.electacta.2018.01.194
45. Wang H, Shi X, Zhang W, Yao S (2017) One-pot hydrothermal synthesis of flower-like β-$Ni(OH)_2$ encapsulated by reduced graphene oxide for high-performance supercapacitors. J Alloys Compd 711:643–651. https://doi.org/10.1016/j.jallcom.2017.04.035
46. Zhou Q, Cui M, Tao K, Yang Y, Liu X, Kang L (2016) High areal capacitance three-dimensional Ni@$Ni(OH)_2$ foams via in situ oxidizing Ni foams in mild aqueous solution. Appl Surf Sci 365:125–130. https://doi.org/10.1016/j.apsusc.2016.01.020
47. Tian Y, Yan J, Huang L, Xue R, Hao L, Yi B (2014) Effects of single electrodes of $Ni(OH)_2$ and activated carbon on electrochemical performance of $Ni(OH)_2$-activated carbon asymmetric supercapacitor. Mater Chem Phys 143:1164–1170. https://doi.org/10.1016/j.matchemphys.2013.11.017
48. Liu M, Tjiu WW, Pan J, Zhang C, Gao W, Liu T (2014) One-step synthesis of graphene nanoribbon–MnO_2 hybrids and their all-solid-state asymmetric supercapacitors. RSC 6:4233–4242. https://doi.org/10.1039/c3nr06650a